Pharm Res (2012) 29:2407–2418
DOI 10.1007/s11095-012-0766-9

RESEARCH PAPER

Surface Functionalization of Mesoporous Silica Nanoparticles Controls Loading and Release Behavior of Mitoxantrone

Amit Wani • Elayaraja Muthuswamy • Galbokka H. Layan Savithra • Guangzhao Mao • Stephanie Brock • David Oupický

Received: 17 December 2011 / Accepted: 24 April 2012 / Published online: 4 May 2012

ABSTRACT

Purpose To investigate the effect of surface functionalization of mesoporous silica nanoparticles (MSN) on crystallization, loading, release and activity of mitoxantrone (MTX).

Methods Thiol-, amine-, and mixed thiol/amine-functionalized MSN were synthesized and characterized by electron microscopy, thermogravimetry, surface area analysis, elemental analysis and zeta potential. MTX loading and release kinetics were determined in phosphate and acetate buffers (pH 7.4 and 4.5). The crystalline state of MTX in MSN was determined by differential scanning calorimetry and X-ray diffraction. Cytotoxicity and activity of MTX loaded MSN were determined by MTS assay in MDA-MB-231 cells.

Results Our results demonstrate that loading of MTX depends strongly on the type of surface functional groups in MSN. Thiol-MSN showed the highest MTX loading (18 % *w/w*) when compared with thiol/amine-MSN (6 % *w/w*) and amine-MSN (1 % *w/w*). MTX release was strongly dependent on the pH of the release medium and the type of surface functional group. MTX was found in the amorphous form when loaded in thiol-functionalized MSN. No significant effect of surface modification of MSN on particle toxicity was observed. MTX loaded in MSN exhibited comparable anticancer activity *in vitro* as free MTX.

Conclusion Surface modifications of MSN have significant effect on MTX crystallization and release behavior.

KEY WORDS drug delivery · drug release · mesoporous silica · mitoxantrone · nanoparticles

ABBREVIATIONS

APTES	3-aminopropyltriethoxysilane
CTAB	*N*-cetyltrimethylammonium bromide
DSC	differential scanning calorimetry
MPTMS	3-mercaptopropyltrimethoxysilane
MSN	mesoporous silica nanoparticles
MTX	mitoxantrone
PBS	phosphate buffered saline
RPMI	Roswell Park Memorial Institute medium
TEOS	tetraethylorthosilicate
TGA	thermogravimetric analysis
XRD	X-ray diffraction.

INTRODUCTION

Therapeutic strategies based on nanoparticle drug delivery systems aim to improve the anti-proliferative activity of anticancer drugs by localizing them in a controlled fashion at the tumor site (1). Mesoporous silica nanoparticles (MSN), such as Mobile Composition Matter number 41

Electronic supplementary material The online version of this article (doi:10.1007/s11095-012-0766-9) contains supplementary material, which is available to authorized users.

A. Wani • D. Oupický (✉)
Department of Pharmaceutical Sciences, Wayne State University
Detroit, Michigan 48201, USA
e-mail: oupicky@wayne.edu

E. Muthuswamy • G. H. L. Savithra • S. Brock
Department of Chemistry, Wayne State University
Detroit, Michigan 48201, USA

G. Mao
Department of Chemical Engineering and Materials Science,
Wayne State University
Detroit, Michigan 48201, USA

(MCM-41), are silica particles containing pores with diameters in the 1.5–20 nm range. MSN have been proposed as a suitable platform for biomedical applications, including drug and gene delivery (2–5). MSN offer several advantages in drug delivery over polymeric nanoparticles, including tunable pore size, large surface area, high drug loading capacity, ability to encapsulate hydrophilic as well as hydrophobic drugs, and easy surface functionalization. Existing evidence suggests that silica materials, including MSN, are biocompatible and bioresorbable (6). Numerous studies described easy hydrolysis and dissolution of porous silica particles in simulated physiologic conditions (7–9). The particles are typically hydrolyzed into silicic acid, which is known to undergo renal elimination *in vivo* (10).

Hydrophobic polymeric nanoparticles efficiently encapsulate hydrophobic drugs but are usually ill suited for encapsulation of large amounts of relatively hydrophilic drugs. Available reports show, for example, that only about 5 % of doxorubicin can be loaded in poly(lactic-co-glycolic) acid nanoparticles (11). In addition, delivery of hydrophilic drugs by hydrophobic polyester nanoparticles is subject to a potentially dangerous dose-dumping. Like polymeric nanoparticles, MSN are able to improve solubility and achieve controlled release of poorly soluble hydrophobic drugs (e.g. camptothecin, paclitaxel) (3,5), attributable to their well-defined porosities and versatile surface chemistry. MSN have also been successfully developed for delivery of water soluble drugs (e.g. doxorubicin.HCl) with an excellent drug loading capacity (~40 % *w/w* loading) (4,12,13). Park *et al.* reported that electrostatic interactions between positively charged doxorubicin and negatively charged porous silica nanoparticles were responsible for the dramatically enhanced loading (14). Controlled release of hydrophilic molecules, such as adenosine triphosphate has been achieved by tailoring the pore size of microporous and mesoporous materials (15). In addition, studies on tuning of pore wall properties such as by silylation of the silica matrix to make it more hydrophobic (16) or amine modification to achieve positively charged surface (17) reveal that release of hydrophilic drugs can be easily adjusted.

Another important aspect of mesoporous silica is amorphization or crystalline-to-amorphous transformation of active pharmaceutical ingredient in the porous nanoconfinement. Mesoporous silica exerts a strong confinement effect on drug crystallization due to its large surface area (greater than 500 m^2/g) with high surface free energy and higher pore volume (e.g., approximately 1 cm^3/g). The small pore size may prevent drug molecule nucleation by preventing the formation of supercritical nuclei beyond critical nucleus size. In addition, the strong adsorption and interaction of drug molecules on the surface of mesoporous silica may also hinder the ordering of drug molecules necessary for crystallization. It has been reported that porous structure has a size-constraint effect on nucleation and crystal growth (18,19). Jacson *et al.* investigated effect of pore size (4 to 73 nm) of porous adsorbent on adsorption of crystalline o-terphenyl and found that crystalline-to-amorphous transformation while decreasing pore size with lowest pore size particles (4 nm) preventing crystallization completely (18).

MTX (Fig. 1) is an anthraquinone derivative that has been extensively investigated for the treatment of breast and prostate cancer but its clinical application has been limited due to severe cardiotoxicity (20). Solid lipid nanoparticles (21), liposomes (22) and polyester nanoparticles (23) have been investigated to improve MTX formulation but limited drug loading capacity and poorly controlled release hindered their utility. Electrostatic interaction of MTX with silica matrix has been reported very recently (24) but systematic investigation of the effect of surface functionalization of MSN on MTX loading and release has not yet been reported. The goal of the present study was to investigate the effect of surface functionalization of mesoporous silica on crystallization behavior of MTX with focus on optimization of surface functionality for achieving amorphous MTX formulations with controlled rate of release. We predicted that surface functionalization of MSN will serve as a simple and robust way of controlling MTX delivery without the need for introducing of any complex mechanism of drug release control into the design of MSN.

MATERIALS AND METHODS

Materials

Tetraethylorthosilicate (TEOS), 3-mercaptopropyltrimethoxysilane (MPTMS), 3-aminopropyltriethoxysilane (APTES), *N*-cetyltrimethylammonium bromide (CTAB), hydrochloric acid, and sulfuric acid were purchased from Sigma-Aldrich (St. Louis, MO). Mitoxantrone dihydrochloride (MTX) was purchased from SantaCruz Biotechnology Inc. (Santa Cruz, CA). Roswell Park Memorial Institute (RPMI), phosphate buffered saline (PBS), fetal bovine serum (FBS) were purchased from Invitrogen (Grand

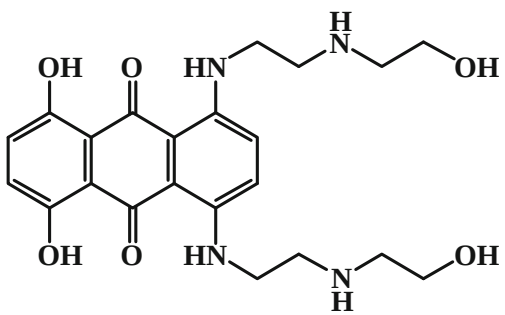

Fig. 1 Chemical structure of MTX.

Island, NJ). Cell titer 96 Aqueous One solution cell proliferation assay (MTS reagent) was purchased from Promega (Madison, WI).

Methods

Synthesis of Mesoporous Silica Nanoparticles (MSN)

SH-, mixed SH/NH_2- (50:50) and NH_2-functionalized MSN were synthesized by co-condensation of TEOS, MPTMS and APTMS using modified surfactant-templated base catalyzed method reported previously (25). In a typical synthesis of mixed SH/NH_2-MSN, 1.0 g of CTAB was dissolved in 480 mL of de-ionized water made basic by the addition of 3.5 mL of 2.0 M NaOH, and the temperature raised to 80 °C. To this solution, 5.0 mL TEOS was injected at a rate of ~1.0 mL/min using a syringe pump while stirring. The injection of TEOS was immediately followed by drop-wise addition of MPTMS (1.3 mmol) and APTES (1.3 mmol), to achieve a molar ratio of TEOS:MPTMS:APTES of 8.7:1:1. The dispersion was maintained at 80 °C for about 2 h and the final product was isolated by centrifugation. The isolated product was washed with excess deionized water and methanol and dried in vacuum. Removal of the CTAB template was carried out by refluxing the dried product in acidic methanol solution (18 mL of 12 M HCl, 20 mL of methanol) overnight. The particles were isolated by centrifugation, washed with methanol and de-ionized water, and dried overnight under active vacuum in a dessicator to yield a free flowing white powder. Synthesis of SH-MSN and NH_2-MSN was carried out using the same procedure using either 2.6 mmol of MPTMS or 2.6 mmol APTES alone.

Characterization of MSN

The morphology and size of nanoparticles were characterized by transmission electron microscopy (TEM) on a JEOL 2010 Analytical Electron Microscope at 200 kV. TEM samples were prepared by placing a drop of a sonicated aqueous solution of MSN on a carbon-coated copper grid. The surface area, average pore size, cumulative pore volume, and pore size distributions were determined from nitrogen adsorption/desorption isotherms acquired at 77 K using a 30 s equilibrium interval on an ASAP 2010 Micromeritics porosimeter. The surface areas were computed using the Brunauer-Emmett-Teller (BET) model. The cumulative pore volumes and the pore size distribution was obtained from density functional theory (DFT) modeling using the DFT package of the Micromeritics V2.00 software over the entire range of the adsorption isotherm. The content of thiol and amino groups in the MSN was determined from the sulfur and nitrogen content in MSN measured by elemental analysis (Atlantic Microlabs Inc., Norcross, GA).

MTX Loading

In a typical experiment, 667 μL of 4.5 mg/mL of MTX in PBS (pH 7.4) was added to 10 mg of dry MSN. The mixture was sonicated for 30 min and kept stirring on a magnetic stirplate for 24 h. Then, drug loaded particles were centrifuged at 14,100 g for 10 min. After centrifugation, MTX loaded MSN were vacuum dried overnight. The amount of MTX loaded in MSN was estimated from the MTX concentration difference in the original solution and the supernatant after loading in MSN. MTX concentration was determined by absorbance at 658 nm. Drug loading is expressed as % w/w=100*(weight of MTX in MSN)/[(weight of MTX in MSN) + (weight of MSN)]. The content of MTX in MSN was also determined by thermogravimetric analysis (TGA) under air (Perkin-Elmer Pyris 1, 10 °C/min), subtracting the mass lost during analysis of empty modified MSN particles.

Zeta Potential Measurement

The measurement of zeta potential of SH-MSN, SH/NH_2-MSN, and NH_2-MSN with and without MTX loading was performed using a ZetaPlus Particle Size and Zeta Potential Analyzer (Brookhaven Instruments) equipped with a 35-mW solid state red laser (658 nm) at 25 °C. Scattered light was detected at 90°. Samples were prepared by suspending 200 μg of particles in 2 mL PBS (pH 7.4). Zeta potential values were calculated from measured velocities using the Smoluchowski equation and results are expressed as the mean ± S.D. of 5 runs.

In Vitro Release of MTX

Release of MTX from MSN was analyzed by suspending a known mass of the particles in 2 mL of appropriate release medium (PBS, pH 7.4, or 0.2 M sodium acetate buffer, pH 4.5). At each pre-determined time point, MSN were centrifuged at 14,100 g for 10 min. One mL of supernatant was removed and replaced with 1 mL of fresh release media. The media volumes and drug concentrations were selected so that sink conditions were maintained during the entire experiment. The concentration of MTX in the supernatant was determined from absorbance at 658 nm using a standard absorbance *vs.* concentration curve constructed for MTX in the corresponding release buffer. Because only 1 mL of the release media was removed at each time point, the amount of released MTX was corrected for MTX remaining in the release medium from the previous time point.

Characterization of Crystalline/Amorphous State of MTX in MSN

The crystalline state of MTX loaded in MSN was determined by differential scanning calorimetry (DSC) and X-ray powder diffraction (XRD). In the DSC analysis, 3–4 mg of sample was packed in hermetically sealed aluminum pans and heated under dry nitrogen purge using MDSC Model 2920 (TA instruments, New Castle, DE) equipped with a refrigerated cooling system. Samples were heated from 0 to 250 °C at a heating rate of 10 °C/minute. Thermograms were analyzed using Universal Analysis 2000 software (TA Instruments, New Castle, DE). The powder XRD patterns were obtained on Rigaku D/MAX-2200PC diffractometer at 40 kV and 40 mA (Cu Kα radiation). Data were obtained from 5° to 30° (diffraction angle 2θ) at a scanning speed of 3°/min at room temperature.

Self-Quenching of MTX Fluorescence in MSN

Effect of MTX loading in MSN on self-quenching of the MTX fluorescence was studied by fluorescence spectroscopy using a Fluoromax-3 (Horiba Jobin Yvon Inc.). 6.9 μg/mL of MTX, either free or loaded in MSN, was suspended in PBS (pH 7.4). The excitation wavelength was set to 607 nm and emission spectra were recorded from 650 to 750 nm.

Cell Culture

Triple negative MDA-MB-231 human breast cancer cell line was a kind gift from Dr. Jing Li, Karmanos Cancer Institute, Detroit MI. The cells were maintained in Hyclone's RPMI medium supplemented with 2.05 mM L-glutamine, 10 % FBS and 1 % penicillin. Cells were maintained in an incubator at 37 °C with 5 % CO_2.

Cell Viability

Cytotoxicity of drug-loaded MSN was determined by the CellTiter 96® Aqueous Cell Proliferation Assay and compared with that of empty MSN. Five thousand MDA-MB-231 cells were seeded in a 96-well plate. One day after reaching confluence, the cytotoxicity of the different surface modified MSN formulations was evaluated by incubating the cells in 100 μL of RPMI/FBS with increasing MSN concentrations. The medium was removed after 72 h and replaced with a mixture of 100 μL fresh RPMI and 20 μL MTS reagent solution. The cells were incubated for 2 h at 37 °C. The absorbance of each well was then measured at 490 nm to determine cell viability. The results are expressed as mean % cell viability relative to untreated cells ± S.D. IC50 values were determined by Prism software using non-linear regression involving log (inhibitor) *vs.* response (three parameters) analysis of dose–response inhibition.

Intracellular Uptake of MTX

Dose dependent cellular uptake of free MTX and MTX loaded in SH-MSN was determined by measuring cell-associated fluorescence of MTX by flow cytometry. MDA-MB-231 cells (2.5×10^5 cells per well) were seeded in 24-well plate 12 h before experiment. Cells were incubated with increasing concentration of free MTX and MTX/SH-MSN in RPMI/FBS for 2 h at 37 °C. Cells were washed twice with PBS and harvested by trypsinization. Cells were resuspended in Hank's buffered salt solution (HBSS) and MTX concentration was analyzed immediately by flow cytometry at an excitation laser wavelength of 658 nm and using a 670 nm emission band pass filter. Flow cytometry analysis was performed on a BD Biosciences LSR II instrument. Ten thousand cells were collected for each measurement. Cellquest software was used for data analysis. Reported fluorescence intensity data were corrected for cell autofluorescence using untreated cells.

Intracellular Release of MTX

Time dependent intracellular release of MTX from internalized SH-MSN particles loaded with MTX was determined by flow cytometry. MDA-MB-231 cells (3.8×10^5 cells per well) were seeded in 12-well plate 12 h before experiment. Cells were incubated with 10 μg/ml of either free MTX or MTX loaded in SH-MSN in RPMI/FBS for 2 h at 37 °C. Cells were washed with PBS to remove any free drug and particles. The cells were then incubated for additional 2, 4 and 6 h in RPMI/FBS and cell-associated fluorescence intensity of MTX was measured by flow cytometry as above.

RESULTS

Synthesis and Characterization of Surface-Functionalized MSN

Surface-functionalized MSN were synthesized by co-condensation of TEOS with the appropriately functionalized siloxane; MPTMS to prepare SH-MSN, APTES to prepare NH_2-MSN or a mixture of MPTMS and APTES to prepare mixed SH/NH_2-MSN. The morphology and pore structure of the modified MSN were first analyzed by TEM (Fig. 2). The TEM images show that all synthesized MSN had a nearly spherical shape with average diameter of 86, 87 and 138 nm for SH-MSN, mixed SH/NH_2-MSN and NH_2-MSN, respectively (Fig S1). The presence of

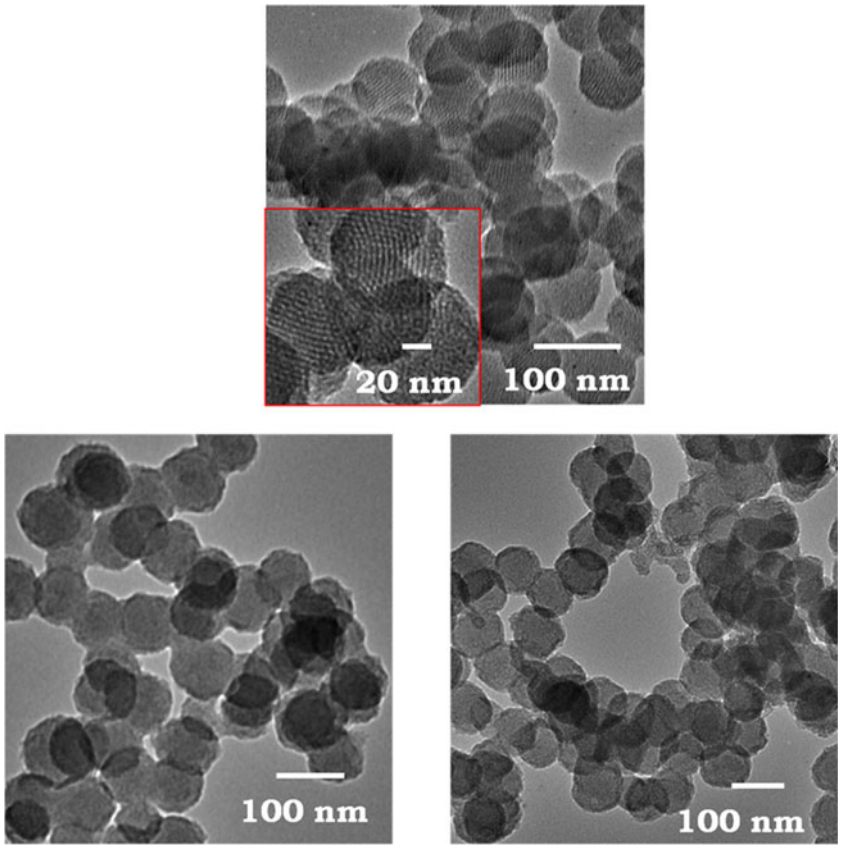

Fig. 2 TEM images of SH-MSN (*top*), NH_2-MSN (*bottom right*) and mixed SH/NH_2-MSN (*bottom left*) (Inset: HRTEM image of SH-MSN).

mesoporous structure in SH-MSN, mixed SH/NH_2-MSN and NH_2-MSN was confirmed by porosimetry (Fig. 3). The nitrogen adsorption/desorption experiments revealed that all the synthesized MSN displayed type IV isotherm, a characteristic feature of mesoporous materials (Fig S2). The main results of the MSN characterization are summarized in Table I. The results demonstrate that surface functionalization had only a limited effect on the pore size and pore volume of the particles. The BET surface area of the SH-MSN and SH/NH_2-MSN was higher than surface area of the NH_2-MSN particles.

The presence of thiols and amines in the MSN was confirmed by elemental analysis. The elemental composition of the functionalized MSN is given in Table II. As expected, no nitrogen was detected in SH-MSN while no sulfur was detected in NH_2-MSN. The elemental analysis results indicate that SH-MSN contained 1.2 mmol of SH/g of MSN, mixed SH/NH_2-MSN contained 0.75 mmol SH/g of MSN and 0.8 mmol NH_2/g of MSN, and NH_2-MSN contained 1.8 mmol NH_2/g of MSN.

The presence of the functional groups had a pronounced effect on the surface charge of MSN (Fig. 4). At neutral pH, NH_2-MSN had an overall positive surface charge with zeta potential 15.6 mV, while SH-MSN exhibited a negative surface charge with zeta potential −15 mV. As expected, the mixed SH/NH_2-MSN showed intermediate zeta potential of 5.2 mV. Zeta potential increased at pH 4.5 with NH_2-MSN, SH-MSN, and SH/NH_2-MSN showing zeta potential of 31.0 mV, −2.5 mV and 16.6 mV, respectively (Table S3).

MTX Loading

We have encapsulated MTX into the synthesized MSN to determine the effect of surface functionalization on MTX loading. The data show that modification of MSN with amino groups limited MTX loading to 1 % *w*/*w*. In contrast, modification of MSN with thiols resulted in significant enhancement of MTX loading to 18 % *w*/*w* (Fig. 5). MSN modified with both thiols and amines exhibited intermediate MTX loading (6 % *w*/*w*). Corresponding encapsulation efficiencies in SH-MSN, SH/NH_2-MSN and NH_2-MSN particles were 60 %, 27 % and 3.4 %, respectively. The differences in MTX loading among the different functionalized MSN were confirmed by TGA (Fig. 6). MTX alone decomposed fully at temperatures above 600 °C. MSN that were not loaded with MTX showed weight loss in the range of 13 to 25 % due to incomplete condensation of TEOS and presence of residual solvents. Comparison of the weight loss of the MTX-loaded MSN with the weight loss observed for the empty particles suggested that the SH-MSN particles

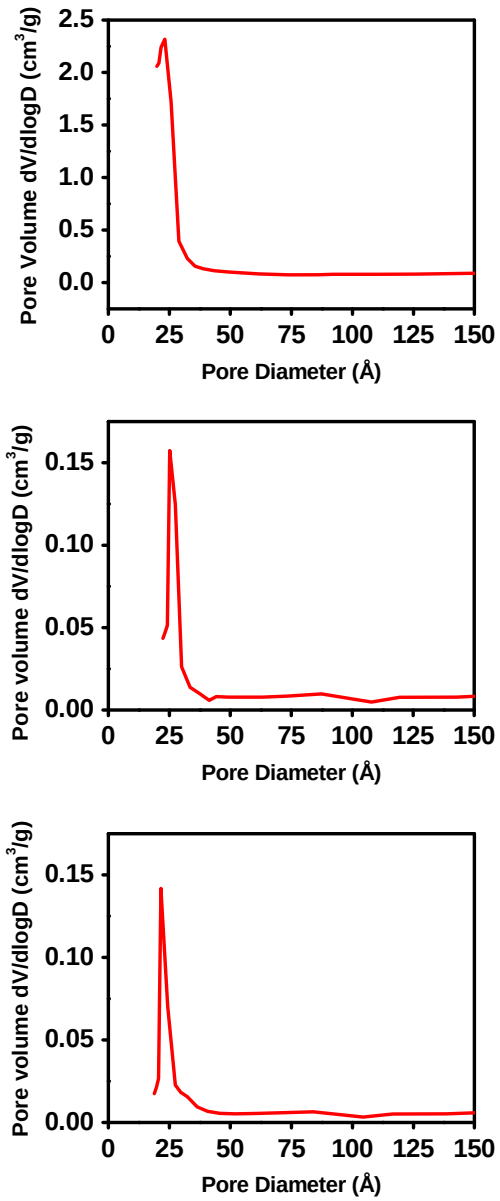

Fig. 3 DFT pore size distribution of surface modified MSN. SH-MSN (*top*), mixed SH,NH_2-MSN (*middle*) and NH_2-MSN (*bottom*).

contained 21 % *w*/*w* MTX, while the mixed SH/NH_2-MSN particles contained 8 % *w*/*w* MTX and the NH_2-MSN particles contained only 1 % *w*/*w* MTX.

Table I Surface Properties of SH-MSN, Mixed SH/NH_2-MSN and NH_2-MSN

MSN	Pore Size (Å)	Pore volume (cm^3/g)	BET S.A. (m^2/g)[a]
SH-MSN	37	0.51	776
SH/NH_2-MSN	28	0.53	754
NH_2-MSN	37	0.57	506

[a] BET: Brunauer-Emmett-Teller surface area measurement

Table II Elemental Analysis of Surface-Modified MSN

Element	Element content (%)		
	SH-MSN	SH/NH_2-MSN	NH_2-MSN
C	4.3	6.4	8.2
H	4.9	2.2	2.8
N	0.0	1.1	2.5
S	4.0	2.4	0.0

Characterization of MTX-Loaded MSN

MSN loaded with MTX were characterized for particle size, zeta potential, morphology, and physical state. TEM studies indicated that after MTX encapsulation, nanoparticles retained spherical morphology; however, filled pores were observed with SH-MSN (data not shown). Loading of the positively charged MTX increased the zeta potential of all the MSN (Fig. 4). Upon MTX loading, the zeta potential of SH-MSN increased from −15.0 to −7 mV, while the zeta potential of the mixed SH/NH_2-MSN increased from 5.2 to 8.1 mV. Despite low MTX loading, the zeta potential of NH_2-MSN increased from 15.6 to 32.1 mV. In acidic conditions (pH 4.5), further increase in the zeta potential was observed. The zeta potential of MTX/SH-MSN was 22.0 mV, while the zeta potential of the MTX-loaded mixed SH/NH_2-MSN was 26.5 mV and the zeta potential of MTX/NH_2-MSN was 42.8 mV (Table S3).

MTX is a fluorescent molecule with emission maximum at 685 nm. Concentration-dependent fluorescence quenching is a well-known phenomenon that can be exploited for determining the release of fluorescent molecules from nanoparticles. We measured fluorescence of MTX loaded in the three types of functionalized MSN (Fig. 7). Our result shows that the levels of loading achieved in SH-MSN are sufficient to achieve quenching of MTX fluorescence. The lower loading achieved in the two amine-containing MSN resulted in MTX fluorescence similar to that of the free drug.

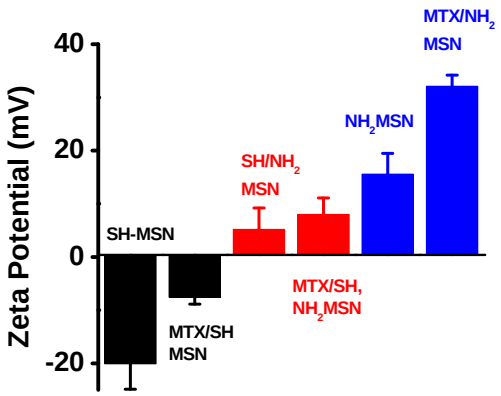

Fig. 4 Effect of surface modification and MTX loading on zeta potential of MSN.

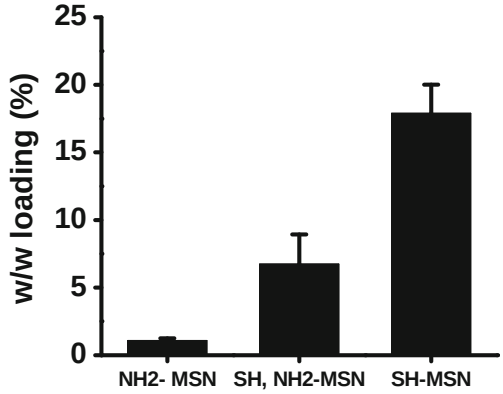

Fig. 5 Effect of surface modification of MSN on MTX loading. (mean ± S.D, n=3).

Drug crystallinity affects the rate of dissolution and release from nanoparticles. We have used DSX and XRD to evaluate crystalline/amorphous state of MTX loaded in MSN. The DSC thermograms of MTX, MTX-loaded MSN, and empty MSN are shown in Fig. 8. Two endothermic peaks (75 and 220 °C) were observed in the sample of free MTX. The peak at 220 °C corresponds to the melting point of dihydrochloride of MTX. The peak at 75 °C represents residual solvent in the commercial sample of MTX. This was confirmed by TGA by observing a small weight loss at that temperature. Analysis of MTX loaded in SH-MSN showed an endothermic peak at 232 °C, which was due to the phosphate buffer used in the loading protocol (Fig. S4). No signs of MTX melting point were observed in MTX-loaded SH-MSN. In contrast, a broad endothermic peak at 188 °C was observed in the sample of MTX loaded in NH_2-MSN. All empty MSN and free MTX showed endothermic signals between 156 °C and 158 °C.

Amorphous nature of MTX loaded in SH-MSN was confirmed by XRD (Fig. 9). Free MTX showed highly crystalline nature as illustrated by the numerous peaks at 5.9, 6.2, 19.4, 23.6, 24.4, 24.9, 25.9, and 26.3°. After encapsulation in SH-MSN no crystalline peaks of MTX were observed. XRD pattern of physical mixture of MTX with MTX-loaded SH-

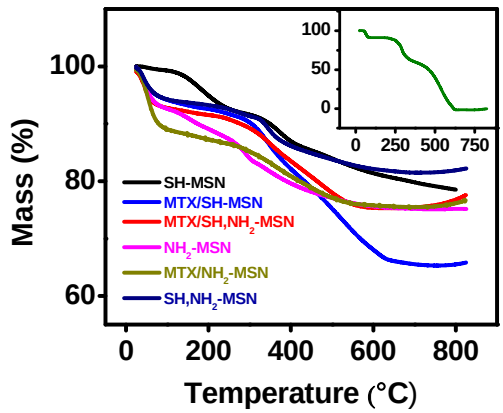

Fig. 6 Thermogravimetric analysis of MSN loaded with MTX. (Inset: TGA of MTX).

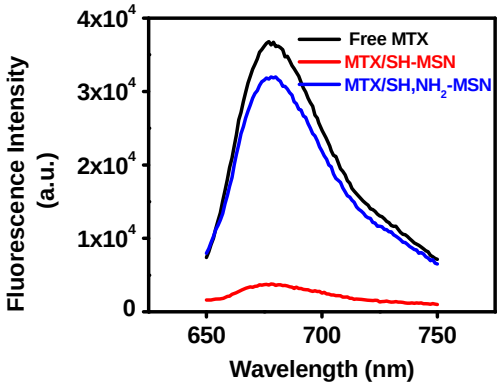

Fig. 7 Fluorescence quenching of MTX loaded in MSN.

MSN showed distinct peaks corresponding to the pure MTX while XRD patterns of control SH-MSN, mixed SH/NH_2-MSN and NH_2-MSN were consistent with amorphous nature of the particles. XRD pattern of MTX loaded in mixed SH/NH_2-MSN revealed non-crystalline state of MTX. NH_2-MSN loaded with MTX showed one crystalline peak at 26.3° while other MTX crystalline peaks were not observed indicating presence of semi-crystalline MTX in NH_2-MSN.

Effect of pH and Surface Functionality on MTX Release

The release behavior of MTX from the different surface functionalized MSN was investigated in PBS (pH 7.4) and in acidic conditions (0.2 M sodium acetate buffer, pH 4.5) to mimic conditions during intracellular lysosomal trafficking of the particles. Release profile of MTX as a function of pH and surface functionality of MSN are shown in Fig. 10. The rate of MTX release from MSN was strongly dependent on the pH of the release media as well as surface modification of MSN. SH-MSN showed a much faster MTX release at pH 4.5 than pH 7.4. Within the first 4 h ~34 % MTX was released at pH 4.5 while only ~1–2 % MTX was released at pH 7.4 from SH-MSN. In contrast, a significantly faster MTX release was observed from mixed SH/NH_2-MSN with 75 % and 90 %

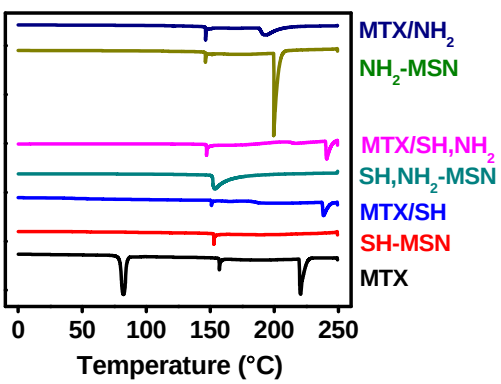

Fig. 8 DSC analysis of MTX-loaded MSN.

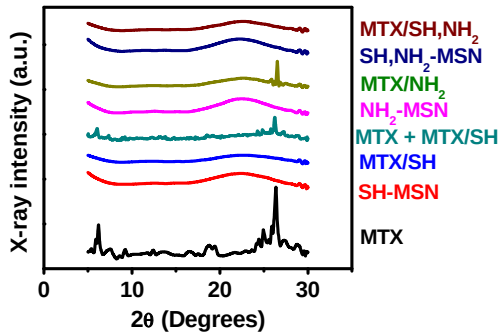

Fig. 9 XRD analysis of MTX-loaded MSN.

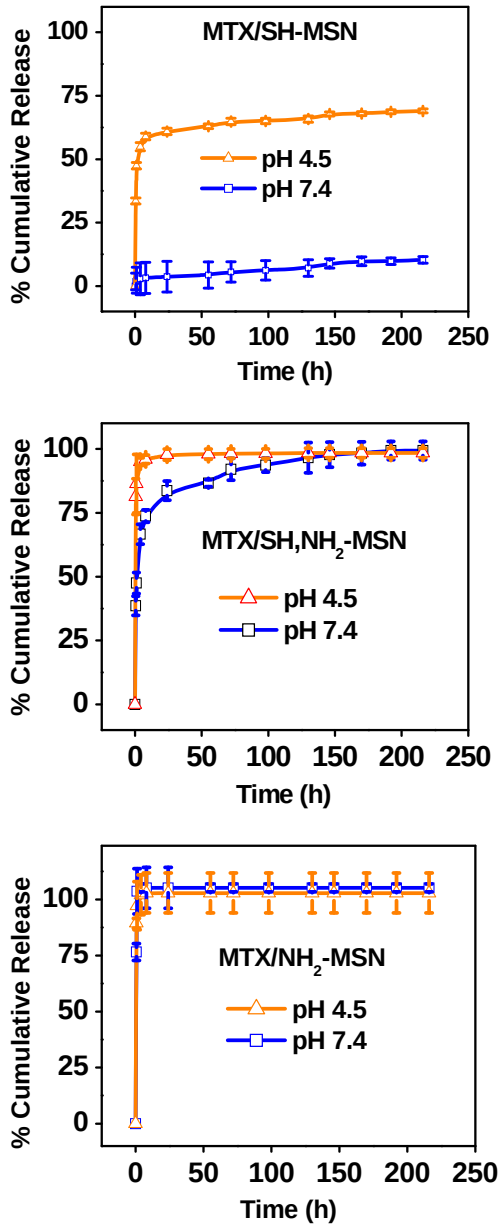

Fig. 10 Effect of pH and MSN surface functionality on the rate of MTX release. (*top*) SH-MSN, (*middle*) SH/NH_2-MSN, (*bottom*) NH_2-MSN. Results shown as mean ± S.D. (n=3).

of the drug released within 4 h at pH 7.4 and 4.5, respectively. MTX was released even more rapidly from NH_2-MSN, with complete release observed within 1 h.

Intracellular Delivery and Release of MTX Using SH-MSN

Dose dependent uptake of free MTX was determined using flow cytometry after 2 h incubation of MDA-MB-231 cells with increasing concentrations of MTX (Fig. 11a). The amount of free MTX in the cells increased continuously in the entire dose range studied. The same assay was used to measure cell-associated fluorescence of MTX delivered by SH-MSN. We found significantly lower fluorescence intensity in case of MTX delivered by SH-MSN when compared with free MTX. Taking advantage of the self-quenching of fluorescence of MTX loaded in SH-MSN (Fig. 7), we then followed MTX fluorescence in cells that were incubated for 2 h with 10 μg/mL of either free MTX or MTX in SH-MSN (Fig. 11b). The medium containing the drug and the nanoparticles was removed and replaced with fresh drug-free medium In case of free MTX, the fluorescence intensity

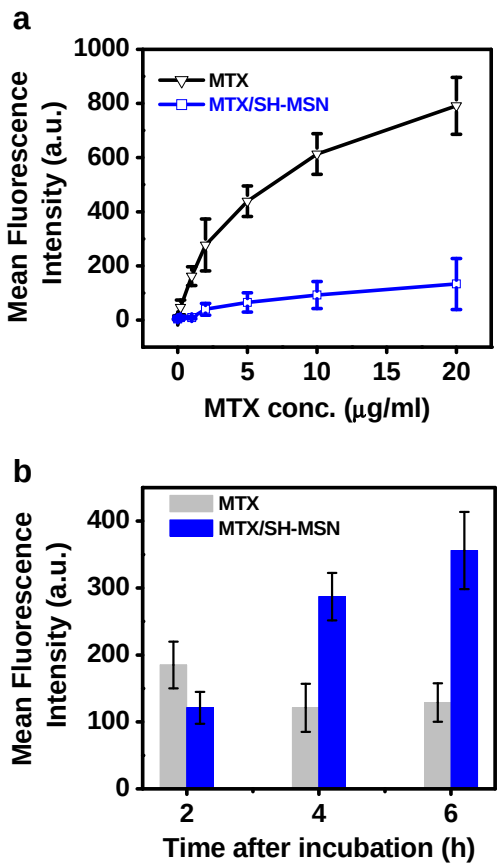

Fig. 11 Flow cytometry analysis to determine (**a**) Effect of MTX concentration on cell uptake and (**b**) Effect of post-incubation time on intracellular content of free MTX.

decreased over the 6 h of observation indicating drug efflux from the cells. During the same time period, the fluorescence intensity in cells treated with MTX/SH-MSN increased almost 3-times. Initially, the intracellular fluorescence intensity of MTX loaded in SH-MSN was low due to quenching (Fig. 7) and the subsequent increase in the fluorescence indicated effective intracellular release of the drug from the internalized particles.

Cytotoxicity of MSN

We have determined the effect of surface functionalization on the cytotoxicity of MSN in MDA-MB-231 (Fig. 12). Cells were incubated with increasing concentration of the different synthesized MSN (from 0.01 μg/ml to 100 μg/ml) and cell viability was assessed by MTS assay. The amine-containing particles had higher toxicity at the highest tested concentration with 83–87 % cell viability, while SH-MSN showed a lower toxicity with 92 % cell viability.

Antiproliferative Activity of MTX Delivered in SH-MSN

Anti-proliferative activity of MTX loaded in SH-MSN was compared with free MTX in a human breast adenocarcinoma cells MDA-MB-231 (Fig. 13). Similar activity was observed for both tested formulations. The concentration of SH-MSN at the highest tested MTX dose was 79 μg/mL. At this concentration, the cell viability of cells treated with empty SH-MSN was 94 % (Fig. 12).

DISCUSSION

Favorable properties, such as large surface area and free volume, make MSN suitable for easy loading of large amounts of a wide range of drugs. The easy way of loading often results in rapid release of drugs and in generally poor control of the drug release from the MSN, severely limiting

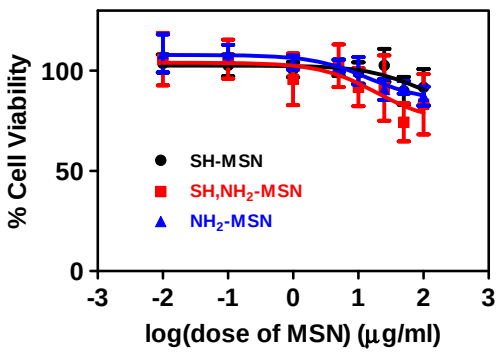

Fig. 12 Effect of MSN surface modification on viability of MDA-MB-231 cells (mean ± S.D., *n*=3).

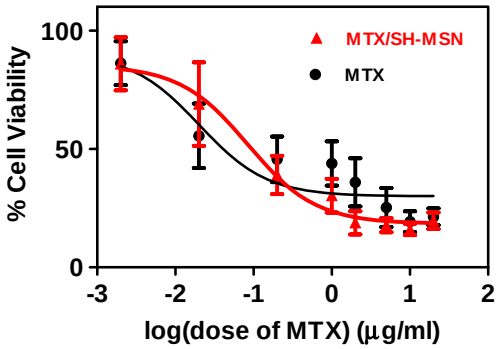

Fig. 13 Anti-proliferative activity of free MTX and MTX loaded in SH-MSN in MDA-MB-231 cells (mean ± S.D., *n*=3).

the potential of MSN in drug delivery. Additional methods of controlling the release are thus required, especially in case of highly soluble drugs with low affinity for silica. Numerous clever and sophisticated strategies have been devised to control the rate of drug release from MSN (26–31). Many of the strategies, however, are not robust enough or compatible with physiologically relevant conditions in which drug delivery vectors must function. In this study, we focused on changes in surface functional groups as a simple way of controlling drug loading and release. We selected MTX as the drug candidate in our studies. MTX exerts antiproliferative activity in advanced breast cancer, acute leukemia, non-Hodgkin's lymphoma and chronic myeloid leukemia by interfering with DNA synthesis through intercalation and stabilization of DNA topoisomerase II cleavable complex (32). Non-specific organ accumulation of MTX justifies development of delivery strategies that can achieve improved delivery to the tumors.

Encapsulation of drugs in MSN is governed by the interplay among drug-solvent, solvent-solvent, drug-silica and silica-solvent interactions. We have initially investigated MTX loading in organic solvents (e.g., DMSO, CH_2Cl_2, DMF, methanol) and mixtures of solvents (e.g., DMF:DMSO 1:0.1, ethanol:water 1:1, methanol:water 1:1) but none of the experiments resulted in drug loading above 4 % *w*/*w*. We have found that loading MTX in aqueous pH-controlled environment provided us with substantially higher levels of loading compared with organic solvents. MTX is a weakly basic drug with two types of secondary amines with pK_a=5.99 and 8.13 and its loading in MSN is thus strongly affected by surface charge of MSN and the pH of the loading media. We have investigated MSN modified with thiols and amines as a way of examining the effect of surface charge on drug loading and release. Thiol-modified MSN are often used in drug delivery applications because of their compatibility with standard bioconjugation techniques to introduce additional functionality into the particles (33). The SH-MSN particles maintained a strong negative charge observed also for the unmodified MSN and caused by the silanol and thiol surface

groups. Surface modification with amines resulted in an overall positive charge of the particles. In order to be able to discern the effect of surface functionalization, we have prepared particles with similar physicochemical properties.

As expected, we have found that MTX loading was strongly influenced by the pH. Negligible MTX loading (~1 % *w*/*w*) was observed in acidic solution (pH 2.0) regardless of the type of surface functionalization of MSN. MTX loading increased with increasing pH and reached 18 % *w*/*w* at pH 7.4 in SH-MSN. Our results are in agreement with a recent report on the effect of pH on MTX loading in MSN (24). Considering that the pK_a of mesoporous silica is ~7 (24), these results suggest that the pH-dependence of MTX loading is mainly controlled by the ionization of the surface silica in the particles. The importance of electrostatic interactions on silica drug loading of another weak base drug, doxorubicin, was reported previously (12).

Surface functionalization of MSN controls drug loading as well as drug release rate. Vallet-Regi *et al.* found that ibuprofen loading was higher in non-functionalized MCM-41 silica compared to amine modified silica (34). Similar trend was observed for erythromycin where non-functionalized silica loading was 34 % compared to 15 % for hydrophobically modified silica (35). We have investigated the effect of surface functionalization on MTX loading using PBS (pH 7.4) as the loading medium. Increasing the relative content of amines in MSN resulted in drastically decreased MTX loading. This observation is in a good agreement with the positive role of electrostatic drug-silica interactions in drug loading. MTX loading increased zeta potential of all MSN, suggesting that at least some of the drug is adsorbed on the surface of the particles. Despite negligible overall loading, the largest increase of zeta potential after MTX loading was observed in NH_2-MSN, suggesting substantial surface adsorption of the drug and thus a limited pore entry. Investigating the physical state of MTX in MSN by XRD and DSC showed that high loading in SH-MSN was not due to MTX crystallization in the pores and that MTX was present in amorphous state. Interestingly, MTX encapsulated in NH_2-MSN showed signs of crystalinity in both DSC and XRD analysis. The observed decrease in melting temperature of MTX loaded in NH_2-MSN is in accordance with the Gibbs-Thompson equation, which predicts the change of melting temperature to vary linearly with the inverse of pore diameter (36). It is likely that electrostatic and hydrogen bond interactions of MTX with the negatively charged silica surface in the pores of SH-MSN inhibits crystallization of loaded MTX (37), while electrostatic repulsion between MTX and NH_2-MSN does not compete with MTX-MTX interactions and supports crystallization. Previously, crystallization of a weakly acidic drug ibuprofen was observed in MSN, supporting the notion that limited interaction between drug and silica surface is favorable for crystallization in the pores (38).

Drug release from MSN can be varied from several hours to several days by altering pore size (17), pore surface area, surface chemistry (39), drug loading (40) and choice of drug molecule (37). Previously, Vallet-Regi demonstrated the feasibility of controlling the release of ibuprofen from MSN by functional groups of silica pore wall (17). The same lab reported that mobility of ibuprofen in the porous silica confinement is dependent on surface functionalization. They found increased mobility for ibuprofen adsorbed on non-functionalized MCM-41 compared to amine–functionalized particles. They attributed faster ibuprofen release rates from non-functionalized silica to the differences in the drug mobility (17). Based on the observed pH-dependence of MTX loading, we hypothesized that surface functionalization will provide a simple method of pH-controlled MTX release from MSN. Indeed, we observed strong pH-dependence of MTX release in SH-MSN (Fig. 10b) with rapid release in acidic pH and very slow release in neutral pH. In comparison, we observed rapid and pH-independent MTX release from NH_2-MSN and to a large extent also from the mixed SH/NH_2-MSN. These differences in the rate of MTX release and its dependence on the pH are due to the differences in the interactions of the drug with the silica matrix. Strong charge-mediated interactions of MTX with negatively charged SH-MSN not only increase the drug loading as discussed earlier but also decrease substantially the rate of drug release. Decrease of ionization of the silica in acidic pH weakens the interactions and facilitates rapid drug release. In the absence of the electrostatic interactions in the NH_2-MSN, the release rate is controlled mainly by the rate of drug dissolution. The strong selectivity of MTX release for acidic pH is a useful feature for drug delivery because it should limit the release in systemic circulation and contribute to rapid release of the drug either in the extracellular acidic tumor microenvironment or in the lysosomes after intracellular uptake (41).

Anticancer activity of drugs encapsulated in nanoparticles is determined by the intracellular concentration of the free drug released from the particles. The self-quenching nature of the fluorescence of MTX loaded in SH-MSN represents a suitable basis for estimating the amount of free, i.e. non-encapsulated, MTX in the cells and the rate of intracellular MTX release from MSN. As shown in Fig. 11a, the amount of free MTX present in cells immediately after incubation is significantly larger when using free drug than when delivering the drug with the particles. The situation changes significantly, however, when the intracellular amount of free MTX is followed after the incubation is stopped and the drug removed from the media (Fig. 11b). Intracellular content of MTX following incubation of cells with free drug declines rapidly after removal of the drug from the media. In contrast, intracellular content of free MTX delivered by the MSN continues to increase even after removal of the particles from the incubation media as the drug is being released from the internalized particles. The

almost three fold increase in cell-associated fluorescence 6 h after incubation is a clear indication of intracellular release of MTX from the particles. MSN are internalized by endocytosis and sequestered in lysosomes (42). The intracellular release of MTX is then triggered by the acidic pH in the lysosomes as suggested by accelerated MTX release rate in acidic pH (Fig. 10). These findings suggest that MSN can deliver MTX into cancer cells and maintain significantly higher intracellular drug concentration than when using free drug.

Evaluation of cytotoxicity of drug delivery carrier is as important as its drug delivery efficiency. *In vitro* toxicity of MSN is known to be highly cell-type dependent and is controlled by the surface area and surface functionality of the particles (43). It has been reported that MSN concentration below 100 μg/ml does not induces cytotoxicity in various cancer cells while growth inhibition is observed when concentration exceeds 200 μg/ml (3,42,44). Our results in MDA-MB-231 cells mostly confirmed prior findings, although we observed enhanced toxicity of the amine-containing nanoparticles at 100 μg/mL when compared with SH-MSN. We then assessed the anti-cancer efficacy of MTX delivered by SH-MSN and found similar activity as free MTX. This finding is not surprising. Many drug delivery systems show little benefit in cell culture where the free drug faces no barriers to delivery, while the particles have to overcome multiple delivery barriers.

CONCLUSION

In summary, this study shows that surface functionalization of MSN can serve as a simple tool to control crystallization, loading and release of water-soluble weak electrolyte drugs like MTX. A thorough investigation of the compatibility of the described mechanism of drug release with *in vivo* conditions as well as determination of the anticancer activity of the described particles in MDA-MB-231 xenograft tumor model *in vivo* are under investigation to further assess the usefulness of MSN in drug delivery.

ACKNOWLEDGMENTS AND DISCLOSURES

We thank Dr. J. Reineke for help with DSC studies and Mr. S. Wang for help with XRD analysis. This work was supported by WSU Bridge funding.

REFERENCES

1. Davis ME, Chen Z, Shin DM. Nanoparticle therapeutics: an emerging treatment modality for cancer. Nat Rev Drug Discov. 2008;7(9):771–82.
2. Slowing II, Vivero-Escoto JL, Wu C-W, Lin VSY. Mesoporous silica nanoparticles as controlled release drug delivery and gene transfection carriers. Adv Drug Deliv Rev. 2008;60(11):1278–88.
3. Lu J, Liong M, Zink JI, Tamanoi F. Mesoporous silica nanoparticles as a delivery system for hydrophobic anticancer drugs. Small. 2007;3(8):1341–6.
4. Chen AM, Zhang M, Wei DG, Stueber D, Taratula O, Minko T, *et al.* Co-delivery of doxorubicin and Bcl-2 siRNA by mesoporous silica nanoparticles enhances the efficacy of chemotherapy in multidrug-resistant cancer cells. Small. 2009;5(23):2673–7.
5. Xia TA, Kovochich M, Liong M, Meng H, Kabehie S, George S, *et al.* Polyethyleneimine coating enhances the cellular uptake of mesoporous silica nanoparticles and allows safe delivery of siRNA and DNA constructs. Acs Nano. 2009;3(10):3273–86.
6. Viitala R, Jokinen M, Tuusa S, Rosenholm JB, Jalonen H. Adjustably bioresorbable sol–gel derived SiO2 matrices for release of large biologically active molecules. J Sol–Gel Part Sci Technol. 2005;36(2):147–56.
7. Galarneau A, Nader M, Guenneau F, Di Renzo F, Gedeon A. Understanding the stability in water of mesoporous SBA-15 and MCM-41. J Phys Chem C. 2007;111(23):8268–77.
8. Lin Y-S, Haynes CL. Impacts of mesoporous silica nanoparticle size, pore ordering, and pore integrity on hemolytic activity. J Am Chem Soc. 2010;132(13):4834–42.
9. Finnie K, Waller D, Perret F, Krause-Heuer A, Lin H, Hanna J, *et al.* Biodegradability of sol–gel silica microparticles for drug delivery. J Sol–Gel Part Sci Technol. 2009;49(1):12–8.
10. Jugdaohsingh R, Reffitt DM, Oldham C, Day JP, Fifield LK, Thompson RPH, *et al.* Oligomeric but not monomeric silica prevents aluminum absorption in humans. Am J Clin Nutr. 2000;71(4):944–9.
11. Park J, Fong PM, Lu J, Russell KS, Booth CJ, Saltzman WM, *et al.* PEGylated PLGA nanoparticles for the improved delivery of doxorubicin. Nanomed Nanotech Biol Med. 2009;5(4):410–8.
12. Meng HA, Liong M, Xia TA, Li ZX, Ji ZX, Zink JI, *et al.* Engineered design of mesoporous silica nanoparticles to deliver doxorubicin and P-glycoprotein siRNA to overcome drug resistance in a cancer cell line. ACS Nano. 2010;4(8):4539–50.
13. Meng H, Xue M, Xia T, Ji Z, Tarn DY, Zink JI, *et al.* Use of size and a copolymer design feature to improve the biodistribution and the enhanced permeability and retention effect of doxorubicin-loaded mesoporous silica nanoparticles in a murine xenograft tumor model. Acs Nano. 2011;5(5):4131–44.
14. Park J-H, Gu L, von Maltzahn G, Ruoslahti E, Bhatia SN, Sailor MJ. Biodegradable luminescent porous silicon nanoparticles for *in vivo* applications. Nat Mater. 2009;8(4):331–6.
15. Slowing II, Trewyn BG, Lin VSY. Mesoporous silica nanoparticles for intracellular delivery of membrane-impermeable proteins. J Am Chem Soc. 2007;129(28):8845–9.
16. Qu F, Zhu G, Huang S, Li S, Qiu S. Effective controlled release of captopril by silylation of mesoporous MCM-41. ChemPhysChem. 2006;7(2):400–6.
17. Munoz B, Ramila A, Perez-Pariente J, Diaz I, Vallet-Regi M. MCM-41 organic modification as drug delivery rate regulator. Chem Mater. 2003;15(2):500–3.
18. Jackson CL, McKenna GB. Vitrification and crystallization of organic liquids confined to nanoscale pores. Chem Mat. 1996;8(8):2128–37.
19. Qian KK, Bogner RH. Application of mesoporous silicon dioxide and silicate in oral amorphous drug delivery systems. J Pharm Sci. 2011;101(2):444–63.
20. van Dalen EC, van der Pal HJH, Bakker PJM, Caron HN, Kremer LCM. Cumulative incidence and risk factors of mitoxantrone-induced cardiotoxicity in children: a systematic review. Eur J Cancer. 2004;40(5):643–52.
21. Lu B, Xiong SB, Yang H, Yin XD, Chao RB. Solid lipid nanoparticles of mitoxantrone for local injection against breast cancer

and its lymph node metastases. Eur J Pharm Sci. 2006;28(1–2):86–95.
22. Law SL, Ho CK, Jang TF, Chang P, Lin FM. Antitumor effect of mitoxantrone-containing liposomes. Int J Pharm. 1996;128(1–2):139–43.
23. Chen HL, Yang WZ, Chen H, Liu LR, Gao FP, Yang XD, *et al.* Surface modification of Mitoxantrone-loaded PLGA nanospheres with chitosan. Colloids Surf, B. 2009;73(2):212–8.
24. Ma YH, Zhou L, Zheng HQ, Xing L, Li CG, Cui JH, *et al.* pH-responsive mitoxantrone (MX) delivery using mesoporous silica nanoparticles (MSN). J Mater Chem. 2011;21(26):9483–6.
25. Bhattarai SR, Muthuswamy E, Wani A, Brichacek M, Castaneda AL, Brock SL, *et al.* Enhanced gene and siRNA delivery by polycation-modified mesoporous silica nanoparticles loaded with chloroquine. Pharm Res. 2010;27(12):2556–68.
26. Ruiz-Hernández E, Baeza A, Vallet-Regí M. Smart drug delivery through DNA/magnetic nanoparticle gates. ACS Nano. 2011;5(2):1259–66.
27. Muhammad F, Guo M, Qi W, Sun F, Wang A, Guo Y, *et al.* pH-triggered controlled drug release from mesoporous silica nanoparticles via intracelluar dissolution of ZnO nanolids. J Am Chem Soc. 2011;133(23):8778–81.
28. Zhu C-L, Lu C-H, Song X-Y, Yang H-H, Wang X-R. Bioresponsive controlled release using mesoporous silica nanoparticles capped with aptamer-based molecular gate. J Am Chem Soc. 2011;133(5):1278–81.
29. Schlossbauer A, Warncke S, Gramlich PME, Kecht J, Manetto A, Carell T, *et al.* A programmable DNA-based molecular valve for colloidal mesoporous silica. Angew Chem Int Ed Engl. 2010;49(28):4734–7.
30. Liu R, Zhang Y, Zhao X, Agarwal A, Mueller LJ, Feng PY. pH-responsive nanogated ensemble based on gold-capped mesoporous silica through an acid-labile acetal linker. J Am Chem Soc. 2010;132(5):1500–1.
31. Knezevic NZ, Trewyn BG, Lin VSY. Functionalized mesoporous silica nanoparticle-based visible light responsive controlled release delivery system. Chem Commun. 2011;47(10):2817–9.
32. Parker BS, Buley T, Evison BJ, Cutts SM, Neumann GM, Iskander MN, *et al.* A molecular understanding of mitoxantrone-DNA adduct formation—effect of cytosine methylation and flanking sequences. J Biol Chem. 2004;279(18):18814–23.
33. Lai CY, Trewyn BG, Jeftinija DM, Jeftinija K, Xu S, Jeftinija S, *et al.* A mesoporous silica nanosphere-based carrier system with chemically removable CdS nanoparticle caps for stimuli-responsive controlled release of neurotransmitters and drug molecules. J Am Chem Soc. 2003;125(15):4451–9.
34. Vallet-Regí M. Ordered mesoporous materials in the context of drug delivery systems and bone tissue engineering. Chem Eur J. 2006;12(23):5934–43.
35. Doadrio JC, Sousa EMB, Izquierdo-Barba I, Doadrio AL, Perez-Pariente J, Vallet-Regi M. Functionalization of mesoporous materials with long alkyl chains as a strategy for controlling drug delivery pattern. J Mater Chem. 2006;16(5):462–6.
36. Ha J-M, Hamilton BD, Hillmyer MA, Ward MD. Phase behavior and polymorphism of organic crystals confined within nanoscale chambers. Cryst Growth Des. 2009;9(11):4766–77.
37. Zhang YZ, Zhi ZZ, Jiang TY, Zhang JH, Wang ZY, Wang SL. Spherical mesoporous silica nanoparticles for loading and release of the poorly water-soluble drug telmisartan. J Control Release. 2010;145(3):257–63.
38. Riikonen J, Makila E, Salonen J, Lehto V-P. Determination of the physical state of drug molecules in mesoporous silicon with different surface chemistries. Langmuir. 2009;25(11):6137–42.
39. Kapoor S, Hegde R, Bhattacharyya AJ. Influence of surface chemistry of mesoporous alumina with wide pore distribution on controlled drug release. J Control Release. 2009;140(1):34–9.
40. Song MR, Li YY, Fai CL, Cui SM, Cui BA. The controlled release of tilmicosin from silica nanoparticles. Drug Dev Ind Pharm. 2011;37(6):714–8.
41. Webb BA, Chimenti M, Jacobson MP, Barber DL. Dysregulated pH: a perfect storm for cancer progression. Nat Rev Cancer. 2011;11(9):671–7.
42. Slowing I, Trewyn BG, Lin VSY. Effect of surface functionalization of MCM-41-type mesoporous silica nanoparticleson the endocytosis by human cancer cells. J Am Chem Soc. 2006;128(46):14792–3.
43. Yu T, Malugin A, Ghandehari H. Impact of silica nanoparticle design on cellular toxicity and hemolytic activity. Acs Nano. 2011;5(7):5717–28.
44. Lu JLM, Li Z, Zink JI, Tamanoi F. Biocompatibility, biodistribution, and drug-delivery efficiency of mesoporous silica nanoparticles for cancer therapy in animals. Small. 2010;6(16):1794–805.